Zigzag structures and domain walls in electroconvection of nematic liquid crystal

H. Zhao and L. Kramer
Universität Bayreuth, Theoretische Physik II, Universitätsstraße 30, D-95440 Bayreuth, Germany
(Received 22 March 2000)

To describe the secondary-bifurcation scenario in ac-driven electroconvection of a planarly aligned nematic liquid crystal layer, we have constructed a generic phase equation coupled to the $\hat{c}$ director. The equations are applicable in particular in the vicinity of the codimension-2 point, where the zigzag and the abnormal roll instabilities meet. This point is also the origin of a line of homoclinic bifurcations, which separates a region where one has stationary zigzag walls from one with spontaneously accelerated abnormal roll walls. The final velocity of the walls depends linearly on the distance from the bifurcation. We analyze the scenario analytically, test it numerically and propose an experimental check.

PACS number(s): 61.30.Gd, 47.20.Ky, 47.65.+a

I. INTRODUCTION

ac-driven electroconvection in planarly aligned nematic liquid crystal layers has become one of the prime examples for anisotropic pattern formation. Over the last decades the rich-threshold and near threshold scenario has been largely clarified (with some interesting exceptions, see, e.g., [1,2]) and much of the interest has shifted to secondary and higher instabilities [3]. From numerical bifurcation analysis of roll solutions in the standard hydrodynamic framework, it has become clear that the first destabilization of the common normal rolls (NRs), which are oriented perpendicular to the alignment axis, occurs with increasing voltage not only through the well-known zigzag (ZZ) instability [4–6], but also through a homogeneous symmetry breaking leading to abnormal rolls (ARs) [7–9]. In the conduction range this occurs at higher frequency. In ARs there is a rotation of the $\hat{c}$ director (projection at midplane of the director $\hat{n}$ onto the cell plane) out of its symmetric orientation perpendicular to the rolls, either to the left or to the right, homogeneously in the cell plane. Because of the planar anchoring the rotation vanishes at the bounding plates, resulting in a twist deformation and making the deformation difficult to detect by the usual optical techniques [10].

The two instabilities meet in a very unconventional codimension-2 (C2) point, where two more lines emerge: a line where ARs restabilize against ZZ modes, and an interesting line of homoclinic (or heteroclinic) bifurcations. We have recently shown that this scenario can be understood from very simple phenomenological equations including only the phase of the roll pattern and the AR mode [11].

Here we will discuss these equations in greater depth and, in particular, present new results concerning the motion of domain walls separating the two versions of ARs. The most interesting feature is that those walls, which below the homoclinic bifurcation (HB) line induce a ZZ configuration, accelerate spontaneously beyond the HB line and settle down at a velocity that depends linearly on the distance from the bifurcation. This is unusual: conventional acceleration instabilities are like pitchfork bifurcations with the velocity proportional to the square root of the distance from the bifurcation point [12]. These domain walls are easily observable [13,14] by the conventional techniques and quantitative experiments on them would be interesting.

These moving domain walls initiate a route to spatiotemporal chaos. As the voltage is increased the walls are created spontaneously, together with defects (dislocations and phase-slip lines). Thus a very anisotropic spatiotemporally chaotic state with structures that are extended in the direction perpendicular to the rolls is established [14]. A description of this state in terms of more general equations where the amplitude of the roll pattern is included, appears promising. Such equations have been derived for electroconvection in homeotropic systems [15,16], but an adaption to planar systems is possible [16].

In Sec. II, we construct the equations valid in the neighborhood of the C2 point at voltage V_{AR} and frequency ω_{AR} and in Sec. III the stability of their homogenous solutions, corresponding to straight rolls, is studied. In Sec. IV, the stationary ZZ solutions are analyzed, leading in particular to the homoclinic bifurcation line. The results are compared with the experiments in a channel geometry [11,17] and the effect of a finite width is considered in Sec. V. In Sec. VI we analyze the traveling domain walls and in Sec. VII we interpret the results, discuss the limitations of the model and relate to convection in homeotropically aligned cells and other systems.

II. THE COUPLED GINZBURG-LANDAU PHASE EQUATIONS

We now construct phenomenological equations in order to describe the system in the vicinity of the C2 point (V_{AR}, ω_{AR}) [7,8,11] (with the voltage V we always denote the RMS of the ac voltage).

Near the AR transition, there are two weakly damped modes, the phase mode of the roll pattern and the $\hat{c}$-director mode. The $\hat{c}$ director can be visualized as the projection of the director at the midplane on the x, y plane. Let ϕ describe the (real) amplitude of the $\hat{c}$-director mode (i.e., an angle) and $\Theta = qx + \theta$ be the phase of the roll pattern, such that $q\hat{x} + \vec{\nabla}\theta$ gives its local wave vector. The transition from NRs to ARs is described most simply by

$$\partial_t \phi = (\mu - g\phi^2)\phi + (K_1\partial_x^2 + K_2\partial_y^2)\phi - \gamma\partial_y\theta, \qquad (1)$$

with positive g, K_1 and K_2. The first expression on the right-hand side (rhs) describes the supercritical pitchfork bifurcation to ARs as μ passes from negative to positive and the second term gives diffusive smoothening by the elasticities. We expect μ to be roughly proportional to $V^2 - V_{AR}^2$. The last term describes an additional torque on the $\hat{c}$ director when the rolls are (slightly) oblique [the local roll angle is $\arctan(\partial_y\Theta/\partial_x\Theta) \approx \partial_y\theta/q$]. This torque acts as a bias on the pitchfork bifurcation. γ must be chosen positive, so reorienting the rolls favors rotation of the $\hat{c}$ director in the opposite sense, as is the case for all the nematics studied [7,8].

The dynamics of the phase modulations is governed by the equation

$$\partial_t \theta = (D_1\partial_x^2 + D_2\partial_y^2)\theta - (\nu + h\phi^2)\partial_y\phi, \qquad (2)$$

with positive D_1, D_2, and h (as it turns out). The first term describes ordinary phase diffusion and the second expression represents the coupling to the $\hat{c}$-director mode. The nonlinear term is essential, because, as we shall see, ν crosses zero at ω_{AR}. We then expect ν to be roughly proportional to $\omega - \omega_{AR}$.

Equations (1) and (2) contain the manifestly dimensionless parameters $h' = \gamma h/(D_2 g)$, $\nu' = \nu\gamma/(|\mu|D_2)$, $K_1' = K_1/D_1$, and $K_2' = K_2/D_2$. It is useful to also consider a rescaled version of the equations by introducing $t = t'/|\mu|$, $x = \sqrt{D_1/|\mu|}x'$, $y = \sqrt{D_2/|\mu|}y'$, $\phi = \sqrt{|\mu|/g}\varphi$, $\theta = (|\mu|/\gamma)\sqrt{D_2/g}\vartheta$, and one obtains

$$\partial_{t'}\vartheta = \partial_{x'}^2\vartheta + \partial_{y'}^2\vartheta - (\nu' + h'\varphi^2)\partial_{y'}\varphi, \qquad (3)$$

$$\partial_{t'}\varphi = K_1'\partial_{x'}^2\varphi + K_2'\partial_{y'}^2\varphi + (\pm 1 - \varphi^2)\varphi - \partial_{y'}\vartheta. \qquad (4)$$

The main assumption underlying the validity of Eqs. (1) and (2) is that a smooth gradient expansion is possible. This can be expected to hold for quasi-1D situations (spatial variations only in x or y, except for linear terms in θ). Otherwise, singular mean-flow contributions are expected to play a role. We will come back to this point in Sec. VII.

Equations (1) and (2) are particularly well founded in situations without variations along x (except for a linear term in θ). Then their derivation from the underlying hydrodynamic equations, including the nonsingular mean flow contributions considered in [7,8], is well established. There are, however, problems with the magnitude of the coefficients, when comparing with experiments (see Sec. V). The solutions we consider here will mostly depend only on y (exception in Sec. VI), so only their stability is influenced by variations along x.

III. HOMOGENEOUS SOLUTIONS AND THEIR STABILITY

Straight-roll solutions (normal or oblique) are characterized by $\phi = \phi_s$ (=const), $\partial_x\theta = Q$ (const), and $\partial_y\theta = P$ (=const), where from Eq. (1)

$$(\mu - g\phi_s^2)\phi_s - \gamma P = 0. \qquad (5)$$

Thus in the case $P = 0$ one has $\phi_s = 0$ (NRs), which is stable against homogeneous perturbations for $\mu < 0$. At $\mu = 0$, NRs lose stability and one has a pitchfork bifurcation generating two branches of ARs with $\phi_s = \phi_{AR} = \pm\sqrt{\mu/g}$. In the case $P \neq 0$ (oblique rolls), one has from the cubic polynomial (5) a real root ϕ_{s1} with $\mathrm{sgn}(\phi_{s1}) = -\mathrm{sgn}(P)$ that varies continuously with μ and is stable against homogeneous perturbations. At $\mu_{sn} = 3(\gamma P g^{1/2}/2)^{2/3}$ there is a saddle-node bifurcation generating two more real roots ϕ_{s2}, ϕ_{s3} with $\mathrm{sgn}(\phi_{s2}) = \mathrm{sgn}(\phi_{s3}) = \mathrm{sgn}(P)$. Choosing $|\phi_{s3}| > |\phi_{s2}|$, the root ϕ_{s3} is stable, the other one unstable.

To test for stability with respect to spatial modulations, we linearize around the straight-roll solutions and calculate the growth rate σ of the modes $\sim e^{\sigma t + \imath(s_x x + s_y y)}$. One finds

$$\sigma = -\frac{1}{2}B + \sqrt{\frac{1}{4}B^2 - C} \qquad (6)$$

with

$$B = -\mu + 3g\phi_s^2 + (K_2 + D_2)s_y^2 + (K_1 + D_1)s_x^2, \qquad (7)$$

$$C = [\gamma\nu - D_2\mu + 3(gD_2 + h\gamma/3)\phi_s^2]s_y^2 + K_2 D_2 s_y^4 + D_1[-\mu + 3g\phi_s^2 + K_1 s_x^2 + (K_2 + K_1 D_2/D_1)s_y^2]s_x^2. \qquad (8)$$

For stability one needs $B > 0$ and $C > 0$. Thus, for NRs ($\phi_s = 0$, $P = 0$), there is, aside from the homogeneous instability at $\mu = 0$ leading to ARs, a long-wave ZZ instability ($s_x = 0, s_y \neq 0$) at

$$\mu = \mu_{zz} = S_{zz}\nu \quad \text{with } S_{zz} = \gamma/D_2. \qquad (9)$$

For negative ν the ZZ instability comes first, and Eqs. (1) and (2) indeed describe the observed crossover scenario, as indicated in Fig. 1(a), lines AR and ZZ. From the expression for C one sees that a nonzero ϕ suppresses the ZZ instability. For negative ν this effect leads to restabilization of ARs above the line

$$\mu = S_{rs}\nu \text{ with } S_{rs} = \frac{S_{zz}}{3S_{zz}/S_{hb} - 2},$$

$$S_{hb} = -3g/h, \qquad (10)$$

see Fig. 1(a), line RS (we introduced S_{hb} for later convenience). Note that $3S_{zz}/S_{hb} = -h'$. The denominator in the expression for S_{rs} could be positive and then the RS line would have a positive slope.

For (slightly) oblique rolls with $\phi = \phi_{s1}$, $P \neq 0$, destabilization still takes place in the form of a ZZ instability ($s_x = 0$). The onset is obtained from the condition

$$S_{zz}\nu - \mu + 3(1 - S_{zz}/S_{hb})g\phi_{s1}^2 = 0, \qquad (11)$$

see dashed line in Fig. 1(a) for $\gamma g^{1/2} P = 0.0011$. In fact, at fixed ν there is an unstable bubble in the μ-P plane [Fig. 1(b); the value $\gamma g^{1/2} P = 0.0011$ is indicated by the dashed line]. The half width P_{max} of the bubble is given by $\gamma g^{1/2} P_{max} = 2(2 - 3S_{zz}/S_{hb})^{-1/2}(-S_{zz}\nu/3)^{3/2}$.

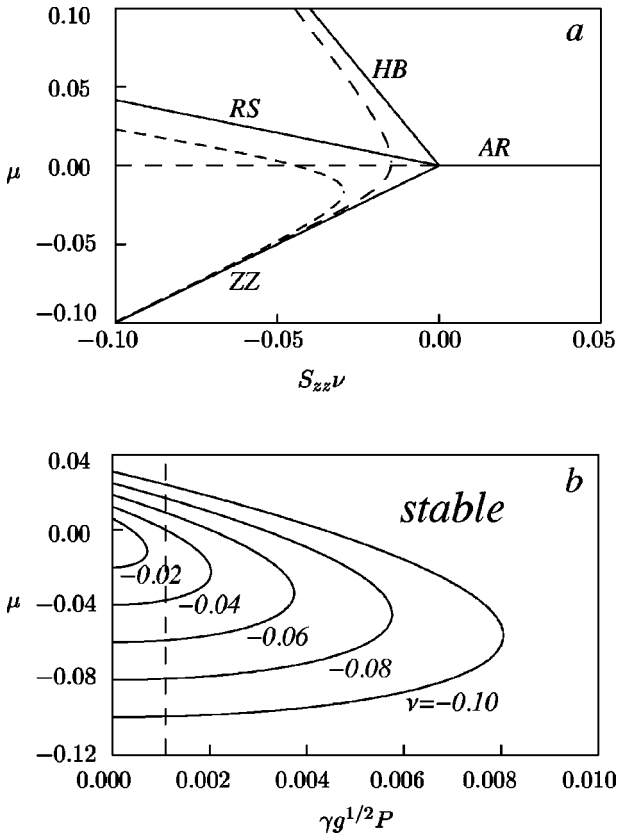

FIG. 1. (a) Stability diagram for $S_{zz}/S_{hb}=-2/5$. Solid (dashed) lines are for $P=0$ ($\gamma g^{1/2}P=0.0011$); (b) The unstable bubble in the μ-P plane for different values of ν.

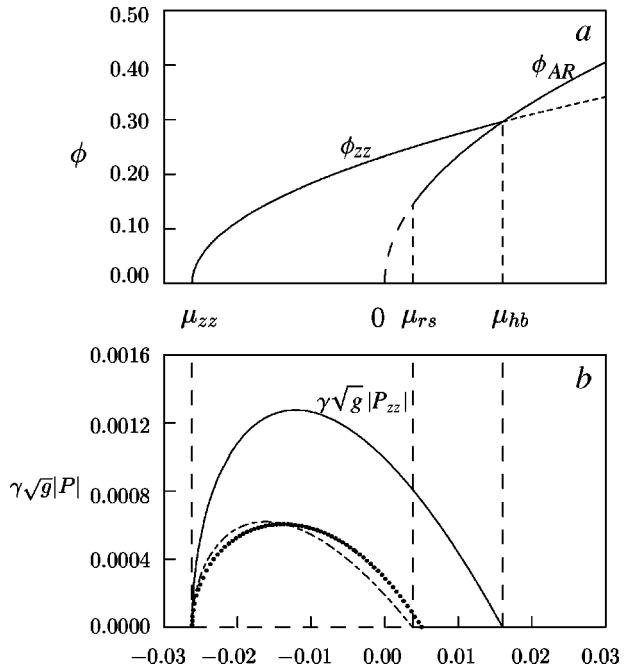

FIG. 2. (a) The $\hat{c}$ director angle ϕ for the heteroclinic ZZ solution and for the (normally oriented) AR; (b) wave number P_{zz} of the oblique roll selected by the heteroclinic ZZ solution for $\nu=0.10$. Also shown is the unstable bubble (dashed line) of oblique rolls. The other parameters $D_2=0.105$, $h=0.0876$, $g=0.182$, and $\gamma=0.0276$ are taken from the hydrodynamics at $\omega=1.0$ [18]. The dotted line shows the unstable bubble including mean-flow effect.

In a more accurate description, the modulation wave vector (s_x,s_y) that destabilizes oblique and abnormal rolls would have a small, but nonzero x component ($s_x\neq 0$) and the unstable bubble would be somewhat larger (see Sec. VII).

IV. THE AR-ZZ SCENARIO

We now analyze the scenario expected when μ is varied for negative ν. We first look for static solutions that depend only on y. Then one has the first integral of Eq. (2),

$$D_2\partial_y\theta-(\nu+h\phi^2/3)\phi=J(=\text{const}). \tag{12}$$

Eliminating $\partial_y\theta$ from Eqs. (1), (12) leads to

$$K_2\partial_y^2\phi=-(\mu-\mu_{zz})\phi+g'\phi^3+S_{zz}J, \tag{13}$$

with $g'=g(1-S_{zz}/S_{hb})$, which can be integrated. Invoking the analogy of a point particle (coordinate ϕ, time y) one sees that the bounded solutions are either constant (straight rolls) or periodic (undulated rolls). Without the appearance of defects the average orientation of rolls cannot change, so the average of $\partial_y\theta$ in the undulated rolls remains that of the straight rolls ($=P$) they were born from. From Eq. (12) one then has $J=D_2P-\langle(\nu+\frac{1}{3}h\phi^2)\phi\rangle$ ($\langle\cdots\rangle$ is the spatial average).

First we look for ZZ solutions in the case $P=\langle\partial_y\theta\rangle=0$, where ϕ oscillates symmetrically around zero ($J=0$). From Eq. (13) one gets a one-parameter family of periodic solutions above the ZZ line (apart from phase shifts) with wave number p between zero and $p_{max}=\sqrt{(\mu-\mu_{zz})/K_2}$, which can be expressed in terms of elliptic functions. In particular there is the heteroclinic limit $p\to 0$ where the solution degenerates to a widely spaced array of domain walls given by $\phi=\phi_{zz}\tanh(\alpha y)$ with $\phi_{zz}=\sqrt{(\mu-\mu_{zz})/g'}$, $\alpha=p_{max}/\sqrt{2}$. They separate regions where ϕ approaches the constant solutions $\pm\phi_{zz}$ [Fig. 2(a)] and the roll angle approaches $\mp\arctan(P_{zz}/(q+Q))$ with

$$\gamma g^{1/2}P_{zz}=\frac{S_{zz}}{S_{hb}(1-S_{zz}/S_{hb})^{3/2}}(\mu-\mu_{zz})^{1/2}(\mu-\mu_{hb}). \tag{14}$$

Thus, the domain walls select a member of the oblique-roll family. The angle (and thereby the undulation) first increases with μ and then decreases [Fig. 2(b)], reaching zero at the ''HB line'' [see Fig. 1(a)].

$$\mu=\mu_{hb}=S_{hb}\nu. \tag{15}$$

There ϕ_{zz} coincides with ϕ_{AR} [Fig. 2(a)] and one is left with straight ARs with a (widely spaced) array of domain walls separating regions with opposite director twist. Above this line (and also for positive ν) only moving domain walls appear to exist stably (details will be discussed below).

Therefore, when the line HB is reached, the domain walls annihilate pairwise, and eventually a single-domain AR is established. From now on ARs persist under changes of the parameters until their stability limit is reached. The integration constant J maintains the AR value $-(\nu+\frac{1}{3}h\phi_{AR}^2)\phi_{AR}$

($=0$ at μ_{hb}). Thus, on lowering μ, ARs persist down to the line RS where a discontinuous ZZ instability occurs. There is a relation between the slopes of the three lines through the C2 point, $S_{rs}=S_{zz}/(3S_{zz}/S_{hb}-2)$, which can be fitted with the experimental data [11]. This relation is in fact invariant under the linear mapping that connect the control parameters μ and ν of the model with the experimental control parameters $V^2-V_{AR}^2$ and $\omega-\omega_{AR}$.

Are the periodic solutions in the ZZ domain, i.e. between the ZZ and HB lines, stable? Clearly they are unstable for p near p_{max} because the NRs, where they bifurcate from at $p=p_{max}$, are unstable in this range against $p_{max}/2$ with a manifestly positive growth rate. Thus, presumably all periodic solutions are unstable against coarsening, because a stability boundary toward smaller values of p is not apparent. Such a stability boundary would have to be related to a stationary bifurcation, which does not exist.

In the case $P\neq 0$, the corresponding scenario is shown in Fig. 1(a) (dashed lines). The ZZ instability remains sharp, since translation invariance along y remains intact, but one has $J\neq 0$ and the periodic solutions are asymmetric. In the heteroclinic limit J approaches zero, so that the roll angles are again determined from Eq. (14), but now the two arms have different length. Approaching the HB line, which is determined from $P_{zz}=|P|$, the relative length of the shorter arm vanishes.

V. COMPARISON WITH EXPERIMENTS; FINITE WIDTH

The NRs, ARs, and ZZ rolls have been studied experimentally in a fairly narrow cell of dimensions $L_x=315$ μm, $L_y\approx 10\,000$ μm with the rolls oriented parallel to the long scale, and show agreement with the scenario discussed above [11,17]. The slight asymmetry in the observed ZZs indicates that a small, but nonzero wave number P was present, resulting presumably from a small misalignment between the alignment axis of the director and the short axis of the channel.

However, the slopes obtained from the experiments do not agree with those obtained from theory, when the coefficients of Eqs. (1) and (2) are derived from hydrodynamics and taken near the C2 point (V_{AR},ω_{AR}). The slopes obtained in this way vary quite strongly with frequency [18].

The effect of the finite width of the experimental cell (12 roll pairs) is to perturb translation invariance, which can be accommodated in the model by including a (small) damping term $-\alpha\theta$ with $\alpha\sim D_1(2\pi/L_x)^2$ on the rhs of (2),

$$\partial_t\theta=(-\alpha+D_1\partial_x^2+D_2\partial_y^2)\theta-(\nu+h\phi^2)\partial_y\phi. \qquad (16)$$

As a result the ZZ instability sets in at finite wave number p_{zz}. One has

$$\mu=-(\sqrt{-S_{zz}\nu}-\sqrt{\alpha_1})^2,$$

$$p_{zz}=\frac{1}{K_2}\sqrt{\alpha_1}(\sqrt{-S_{zz}\nu}-\sqrt{\alpha_1}), \qquad (17)$$

where $\alpha_1=(K_2/D_2)\alpha$. The restabilization line is characterized by

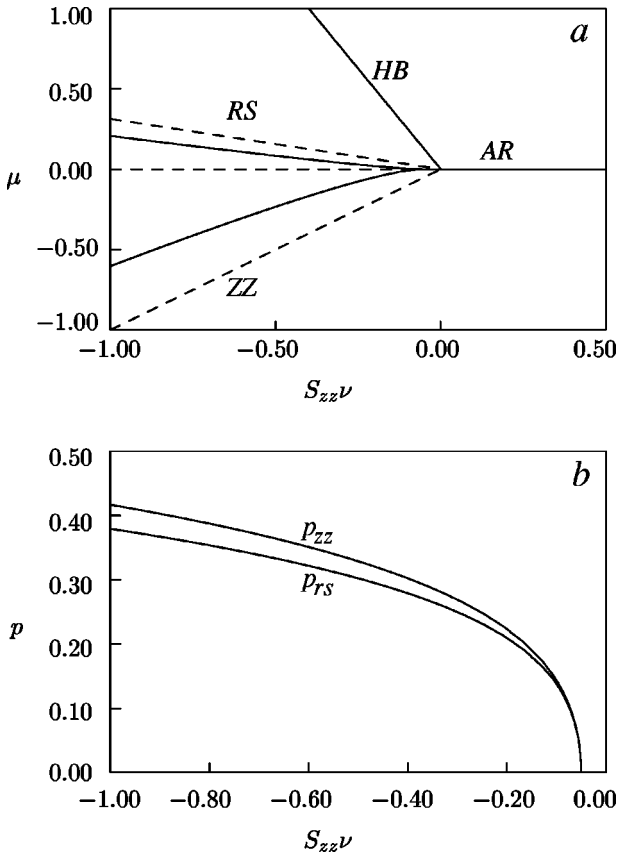

FIG. 3. (a) Stability diagram with the damping term $\alpha=0.1$ (solid); dashed lines pertain to $\alpha=0$; (b) The critical wave numbers at the ZZ instability and on the restabilization line at $S_{zz}/S_{hb}=0.4$, $K_2=1$, $\alpha=0.1$.

$$\mu=\frac{1}{(2-3S_{zz}/S_{hb})^2}\{-(2-3S_{zz}/S_{hb})(\alpha_1+S_{zz}\nu)+4\alpha_1 - \sqrt{8\alpha_1[2\alpha_1-(2-3S_{zz}/S_{hb})(\alpha_1+S_{zz}\nu)]}\},$$

$$p_{rs}=-\frac{1}{K_2(2-3S_{zz}/S_{hb})} \times\{2\alpha_1-\sqrt{2\alpha_1[2\alpha_1-(2-3S_{zz}/S_{hb})(\alpha_1+S_{zz}\nu)]}\}. \qquad (18)$$

This does not change the topology of the scenario, but the C2 point is moved to $\mu=0$, $\nu=-\alpha_1/S_{zz}$. The slopes of the ZZ and RS lines become zero at the C2 point and the critical wave number goes to zero there. The HB line is unchanged. In Fig. 3, we have plotted the stability diagram and the critical undulation wave number p_c for the damping $\alpha=0.1$. The finite wavelength of the ZZ undulations observed in the experiment presumably results from this effect.

VI. TRAVELING DOMAIN WALLS

In the following we return to the unperturbed Eqs. (1), (2). Since for $P=0$ the NR to AR transition corresponds to a pitchfork bifurcation, one has coexistence of symmetry-degenerate states. One then expects the existence of stationary domain walls separating the states. Obliqueness of the

rolls acts as a bias and renders the bifurcation imperfect. For $\gamma g^{1/2}|P|<\gamma g^{1/2}P_{max}=\sqrt{\frac{4}{27}}\mu^{3/2}$, i.e., for not too large roll angle, there still remain two stable asymmetric abnormal roll solutions, and traveling domain walls are expected to exist. We will show that the situation is actually more complicated.

For the analysis of this problem we use the scaled Eqs. (3) and (4). We look for solutions where the wave vector of the rolls is the same on both sides of the wall. We first separate out from the phase ϑ all linear terms, i.e. we write $\vartheta = Q'x' + P'y' + \overline{\vartheta}$, where $\overline{\vartheta}$ can now be assumed to be bounded. In order to allow for domain walls of different orientations we rotate the coordinate system, $x' = \xi\cos\alpha - \zeta\sin\alpha$, $y' = \xi\sin\alpha + \zeta\cos\alpha$ and consider solutions $\overline{\vartheta}$ and φ that depend only on one space variable (we choose ζ). Then Eqs. (3), (4) reduce to

$$\partial_{t'}\overline{\vartheta} = \partial_\zeta^2\overline{\vartheta} - (\nu' + h'\varphi^2)\cos\alpha\,\partial_\zeta\varphi, \tag{19}$$

$$\partial_{t'}\varphi = K\partial_\zeta^2\varphi + (1-\varphi^2)\varphi - \cos\alpha\,\partial_\zeta\overline{\vartheta} - P', \tag{20}$$

with $K = K_1'\sin^2\alpha + K_2'\cos^2\alpha$. We look for solutions that depend only on $\eta = \zeta - Vt'$, so that

$$\partial_\eta^2\overline{\vartheta} + V\partial_\eta\overline{\vartheta} - (\nu' + h'\varphi^2)\cos\alpha\,\partial_\eta\varphi = 0, \tag{21}$$

$$K\partial_\eta^2\varphi + V\partial_\eta\varphi + (1-\varphi^2)\varphi - \cos\alpha\,\partial_\eta\overline{\vartheta} - P' = 0. \tag{22}$$

A. Parallel walls

There is the simple case $\alpha = (\pi/2)$ $(\cos\alpha = 0)$ pertaining to walls parallel to normal rolls (perpendicular to the undisturbed director). There the $\hat{c}$ director does not couple to the phase and one is left with the equation

$$K\partial_\eta^2\varphi + V\partial_\eta\varphi + (1-\varphi^2)\varphi - P' = 0, \tag{23}$$

which can be solved exactly by the ansatz $\partial_\eta\varphi = a(1-\varphi_+)\times(1-\varphi_-)$, where φ_+, φ_- are two (real) roots of the polynomial $(1-\varphi^2)\varphi - P' = 0$, which exist for $|P'| < P_0' = 2/3^{3/2}[= (\mu^{3/2}/\gamma g^{1/2})(2/3^{3/2})$ in the original scaling]. In the case where φ_+, φ_- are the stable solutions, one easily finds

$$V = \sqrt{\frac{K}{2}}(\varphi_+ + \varphi_- - 2\varphi_0), \tag{24}$$

where φ_0 is the unstable solution. These walls should exist in the range of stable ARs. The stationary walls, which are of the form $\varphi = \tanh(\eta y/\sqrt{2K})$, have been observed in experiments [7].

We mention that one can also have traveling walls that connect the *unstable* state with one of the stable states. Then one actually has a continuous family of front solutions with different velocities. However, only one front is stable and its velocity is given by either

$$V^* = 2\sqrt{K}(\varphi_+ - \varphi_0)$$

or

$$V^\dagger = \sqrt{\frac{K}{2}}(\varphi_+ + \varphi_0 - 2\varphi_-), \tag{25}$$

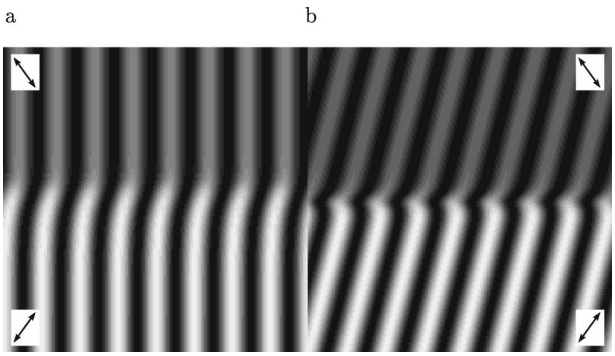

FIG. 4. Snapshots reconstructed from 1D simulations of perpendicular walls moving downward. Across the wall the orientation of the $\hat{c}$ director changes. Double-headed arrows indicate the orientation far from the wall. The gray scales represent $\Phi = (\varphi + 1.5)\cos[q'x' + \vartheta(y')]$ (white: $\Phi = 0$) with the wave number $q' = 0.2$ of the pattern chosen arbitrarily. (a) Wall between ARs parallel to the unperturbed director for $P' = 0$, $\nu' = -0.25$, $h' = 0.9$, $\alpha = 0$ $(\epsilon - \epsilon_0 = 0.05)$, $K = 1$; (b) wall between slightly oblique ARs: $P' = 0.05$, $\nu' = -0.30$, $h' = 0.9$, $\alpha = 0$ $(\epsilon - \epsilon_0 = 0.05)$, $K = 1$.

depending on which is larger [19]. The velocity V^* pertains to the case where the velocity is selected by the leading edge on the unstable side (linear front selection). The other case is actually very similar to the stable-stable wall (nonlinear front selection).

B. Perpendicular walls

Walls with $\cos\alpha \neq 0$ behave very differently. Snapshots of examples from numerical simulations are shown in Fig. 4. From Eq. (21) it follows that for $V \neq 0$ (however small) one has $\partial_\eta\overline{\vartheta} = 0$ at infinity (since $\partial_\eta\varphi = 0$ there), which is consistent with the boundedness of $\overline{\vartheta}$ and expresses phase conservation. Eliminating $\partial_\eta\overline{\vartheta}$ from Eqs. (21) and (22) leads to

$$K\partial_\eta^3\varphi + (1+K)V\partial_\eta^2\varphi + [H(1-3\varphi^2) - \epsilon + V^2]\partial_\eta\varphi + V[(1-\varphi^2)\varphi - P'] = 0, \tag{26}$$

where $H = 1 + \frac{1}{3}h'\cos^2\alpha$ and $\epsilon = (\nu' + \frac{1}{3}h')\cos^2\alpha$.

The boundary conditions are

$$\varphi \to \varphi_\pm \text{ for } x' \to \pm\infty, \tag{27}$$

where $\varphi_\pm$ correspond to stable ARs [the solutions of $(1-\varphi^2)\varphi = P'$]. One expects a unique solution that fixes V as a nonlinear eigenvalue.

For $V = 0$, i.e., on the HB line, Eq. (26) can be integrated (we set $\epsilon = \epsilon_0$ on the HB line),

$$K\partial_\eta^2\varphi_0 + [H(1-\varphi_0^2) - \epsilon_0]\varphi_0 = 0. \tag{28}$$

This equation is the equivalent of Eq. (13) in reduced units and with the integration constant chosen zero, as is appropriate on the HB line. One easily finds

$$\epsilon_0(P') = -H^{3/2}/(1-\nu')^{1/2}|P'|. \tag{29}$$

From Eq. (26) we expect the velocity to depend linearly on $\epsilon - \epsilon_0$, so we write

$$\varphi=\varphi_0+\varphi_1 V+\cdots, \quad \epsilon=\epsilon_0+\epsilon_1 V+\cdots, \tag{30}$$

which leads at first order in V to

$$\partial_\eta L\varphi_1=\epsilon_1\partial_\eta\varphi_0-(1+K)\partial_\eta^2\varphi_0-[(1-\varphi_0^2)\varphi_0-P'], \tag{31}$$

with the linear operator

$$L=K\partial_\eta^2+H(1-3\varphi_0^2)-\epsilon_0. \tag{32}$$

For small P' the last term in Eq. (31) can be replaced by $-(K/H)\partial_\eta^2\varphi_0$ [see Eq. (28)], and then Eq. (31) can be integrated to give

$$L\varphi_1=\epsilon_1\varphi_0-[(1+K)-K/H]\partial_\eta\varphi_0+C. \tag{33}$$

The constant C is to be chosen such that $\varphi_1=0$ behind the wall ($x\to-\infty$ for $V>0$), i.e. at leading order $C=\epsilon_1$ (we choose $\varphi_0\approx-1$ for $x\to-\infty$). Then $-(2H+\epsilon_0)\varphi_1\to 2\epsilon_1$ at the tip of the wall. This might seem like a contradiction with the boundary conditions (27), which actually require $\varphi_1\to 0$ on both sides (since φ_0 already satisfies the correct boundary conditions). However, one sees from Eq. (26) that at the tip there is a slow decay over the length

$$\lambda=-\frac{2}{2H+\epsilon}V, \tag{34}$$

which is not included in the φ_1 obtained from Eq. (33). In principle one can determine the full φ_1 by an asymptotic matching procedure, but it is much simpler to determine V via a solvability condition by invoking the fact that the translation mode $\partial_\eta\varphi_0$ is a zero-eigenvalue solution of L. Then, at lowest order, the slowly decaying part of φ_1 is not needed.

Multiplying Eq. (33) by $\partial_\eta\varphi_0$ and integrating from $-\infty$ to $+\infty$ gives

$$\epsilon_1=\frac{\epsilon-\epsilon_0}{V}=\frac{1}{3}\sqrt{\frac{2H}{K}}(1+K-K/H), \tag{35}$$

where we have used $\int_{-\infty}^{\infty}d\eta\,\partial_\eta\varphi_0=2$ and $\int_{-\infty}^{\infty}d\eta(\partial_\eta\varphi_0)^2\approx\int_{-1}^{+1}d\varphi\sqrt{H/2K}(1-\varphi^2)=\frac{4}{3}\sqrt{H/2K}$ at lowest order in P'. This then is the desired result for the velocity V. The comparison of this formula with numerical results is shown in Fig. 5.

Now coming back to the phase $\overline{\vartheta}$ of the rolls we observe from Eq. (21) that there is a phase shift across the wall, which is given by

$$\Delta\overline{\vartheta}=2\frac{\epsilon-\epsilon_0}{V}. \tag{36}$$

This phase shift accumulates at the front of the wall. At leading order, the phase shift is independent of ϵ [see Eq. (35)]. In Fig. 6(a) we show a simulation of Eqs. (3) and (4) for $P'=0$, $\epsilon=0.05$ with initial conditions that initiate an evolution toward a static, symmetric ZZ wall. Since such a wall is unstable for $\epsilon>0$ there eventually occurs a symmetry breaking (here induced by numerical noise), so that a traveling wall is formed (here traveling upward). The phase shift and the slow decay in the front part of the wall can be seen.

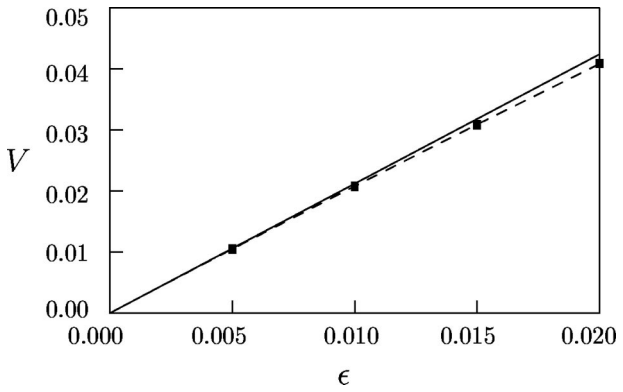

FIG. 5. Comparison of analytical and numerical velocity of walls for $h'=0$, $P'=0$, $\alpha=0$, i.e. $\epsilon=\nu'$, $K=1$; solid line, analytical result; dashed line, numerical solution of the nonlinear eigenvalue problem (26),(27); points, numerical simulations of Eqs. (3) and (4) in 1D.

In Fig. 6(b) the wall velocity is shown as a function of time (for the momentary position we took the zero of φ). After a rather long time delay there is an exponential growth (exponent σ), an overshoot, and an exponential relaxation into the steady state. The numerically determined growth exponent could be fitted in the range $0.002<\epsilon<0.05$ (other parameters as in Fig. 6) accurately by $\sigma=0.000\,012+0.8322\epsilon^{1.834}$. Moreover we found that the complete curves $V(t')$ for different ϵ collapse to a single curve by measuring times in units of $1/\sigma$ and V in units of $\epsilon-\epsilon_0$. We have (as yet) no explanation for this result.

The traveling walls are often observed in experiments [13,14], although their velocity has not been studied quantitatively. The phase shift should be experimentally observable.

VII. DISCUSSION AND CONCLUDING REMARKS

A. Discussion

We have presented a study of the vicinity of the C2 point (V_{AR},ω_{AR}) where the ZZ instability crosses over to the AR transition. In our normal-form type model equations the V-ω plane is mapped onto the μ-ν plane, with the C2 point at the origin. The model expresses a generic stability diagram of straight rolls (normal, abnormal and oblique rolls) and ZZ solutions. For $\nu<0$, where NRs are destabilized first by the ZZ instability, there is a bubble of unstable rolls in the μ-P plane. In this range one has ZZ solutions that extend well above the AR instability at $\mu=0$, and terminate in an unusual homoclinic/heteroclinic bifurcation scenario leading from ZZs to ARs. Whereas the existence and stability of straight-roll solutions can be obtained directly from hydrodynamics [7,8,18], it would have been hard to discover the global bifurcation without the simple equations.

A particularly interesting feature is the hysteresis found when the HB line is crossed from above. Then ARs persist down to a well-defined stability limit, the RS line. Such predictions are in agreement with experiments [11,17]. In fact, for many other nematics, like the one considered in Refs. [7,8], the ZZ instability line meets the primary bifurcation line at another significant C2 point (the Lifshitz point) [3], which separates the regimes where oblique and normal rolls

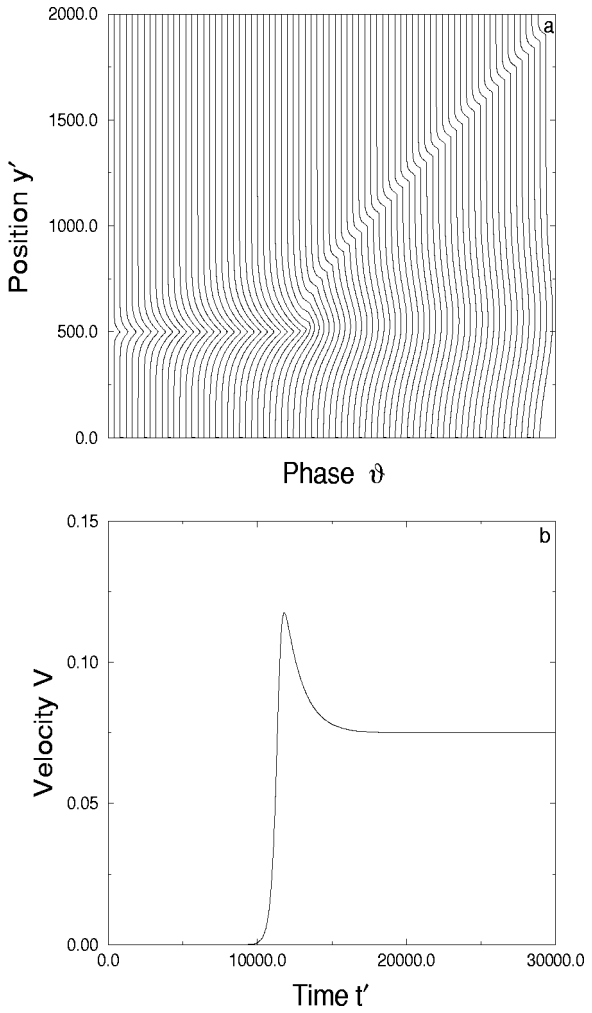

FIG. 6. Simulation of the process of symmetry breaking of a wall for $P'=0$, $\epsilon=0.05$, $h'=0.9$, $\nu'=-0.25$, $\alpha=0$, $K=1$. Initially $\varphi(y')=\tanh(y'/\sqrt{2})$, $\vartheta(y')=0$. (a) Plot of $\vartheta(y')$ for a sequence of times. The time interval between curves is $\Delta t'=400$. Initially $\vartheta=0$. At first a ZZ state develops, which eventually undergoes a symmetry breaking leading to a moving wall. (b) The velocity of the wall as a function of time. At first the velocity increases exponentially, then deceases to a constant.

appear at threshold. The vicinity of this point can be described by a generalized Ginzburg-Landau equation first introduced in [20].

Let us offer an intuitive picture of some aspects of the scenario. Increasing μ the ''abnormal torque'' on the $\hat{c}$ director [first term on the rhs of Eq. (1)] increases. Because of the coupling term proportional to $\gamma\partial_y\theta$, a combined local rotation of the rolls and of the $\hat{c}$ director (in the opposite sense) becomes unstable first if $\nu<0$, i.e., when the director distortion reinforces the roll bending. Thus for $\nu<0$ (and $\gamma>0$) one first has the ZZ instability. We conclude that in the vicinity of the C2 point, the abnormal torque lies at the origin of the ZZ instability (together with positive reinforcement). This is in contrast to the situation near the primary threshold in the vicinity of the Lifshitz point. Here the torque on the $\hat{c}$ director is weak, and the ZZ instability involves only the phase of the rolls.

Restabilization of normally oriented ARs for $\mu>\mu_{rs}$, $\nu<0$ is related to the fact that once the abnormal torque is saturated, there is no driving force left for undulations. The reduction of the heteroclinic roll angle in developed ZZs, and the eventual straightening out at the HB line is of different origin. It arises from the fact that the nonlinear contribution of the term that couples the director to local rotation of the rolls [the term in Eq. (2) proportional to $h(>0)$] counteracts the abnormal-torque effects of Eq. (1) and eventually overcomes the linear contribution [proportional to $\nu(<0)$].

Right on the HB line the ZZ walls degenerate to AR walls that are perpendicular to the normally oriented rolls (or at least roughly so). In this way the HB line can be identified experimentally. Further experimental study of this line would be useful in view of the discrepancies between experiment and hydrodynamical theory mentioned previously. When the voltage and/or frequency is increased further a ZZ in the opposite sense starts to develop. ZZ solutions exist but they are unstable against spontaneous acceleration of the walls, as we have shown in detail (see Fig. 6 for a simulation). Surprisingly, the velocity at which the wall finally settles down (after a rather long transient including an overshoot), depends linearly on the distance from the HB line. It would be interesting to test our prediction by preparing a ZZ wall below the HB line, and observing its acceleration under appropriate voltage and/or frequency changes.

In simulations of Eqs. (1) and (2) with random initial conditions we have not found long-time solutions other than those presented here. Outside the ZZ range (i.e., below the ZZ line, above the HB line and for $\nu>0$) we either find NRs ($\mu<0$) or ARs ($\mu>0$). Between the ZZ and the HB lines, the system typically ends up in a symmetric ZZ state near to the heteroclinic limit.

B. Limitations of the model

Now let us comment on the validity of the model. First of all, it is restricted to the immediate neighborhood of the C2 point and to situations where one has a well-ordered and defect-free roll pattern. Second, when ϕ depends on x one has to allow for a term proportional to $\phi\partial_x\phi$ in Eq. (2), which is of the same order as the last term. It can easily be included in the analysis of the parallel walls in Sec. VI A where it only leads to quantitative corrections. Adding only this term has a qualitative effect on the destabilization of ARs, where it leads to a parallel, upward shift of the restabilization line [RS in Fig. 1(a)], which now does not pass through the C2 point. The modulation wave vector now has a nonzero component s_x in the x direction. The instability thus becomes of skewed-varicose type.

However, when ϕ depends on x and y, one also has to include singular mean flow terms, which destroy the smooth gradient expansion in 2D situations (actually 3D on the hydrodynamic level). For this purpose one has to introduce an additional (static) equation for the mean flow, which couples mainly to the phase equation [18]. One of the effects of the mean flow is to deform the restabilization line, in particular near the C2 point, such that it now passes again through the C2 point. The restabilization line remains above the one of the simple model and the instability remains of the skewed-varicose type.

The singular mean flow also influences the stability of oblique rolls ($P\neq 0$). The bubble of unstable rolls in the μ-

P plane (at fixed $\nu<0$) discussed at the end of Sec. IV is deformed [see Fig. 2(b) for an example], although its width very near to the C2 point still appears to scale approximately with $(-\nu)^{3/2}$. The stability properties of ZZ solutions are presumably also affected by the mean flow.

Let us repeat that these additional terms do not influence the y-dependent solutions discussed here. A detailed study of their effect is beyond the scope of this work.

C. Relation to other systems

Let us comment on the situation in homeotropically aligned cells in materials with negative dielectric anisotropy, where one has electroconvection after a bend-Fréedricksz transition. Without an additional magnetic field in the plane of the layer, one has a direct transition to disorder [15,16,21,22]. However, with a magnetic field one recovers a scenario reminiscent of the one in planar cells. The AR transition has recently been studied quantitatively [23]. In fact, in the limit of small magnetic field, one can deduce from the condition of overall rotational invariance the relation $3S_{zz}/S_{hb}=-h'=2$. As a consequence the restabilization line is vertical [see Eq. (10)] and the HB line is tilted to the right. When the rotation of the $\hat{c}$ director becomes large, disclination lines are formed and more complex patterns arise [23,24].

Our derivation of the normal-form equations indicates that the underlying two-mode scenario can be of general importance, e.g. for certain types of line defects and some types of domain walls in the bend-Fréedricksz distorted state in nematics. Sometimes in these 1D extended structures the director can escape out of the symmetry plane, which may mimic the transition from NRs to ARs described by ϕ. If the position of the line/wall is not fixed from outside it can be described by our phase variable θ. In those cases where one has a potential (no dissipative driving), our model predicts $\gamma\nu<0$ so that the ZZ instability always occurs first, which appears to be consistent with experiments [25–27]. The model is not applicable if the coupling terms between the two active modes vanish by symmetry, as is the case in Ising-Bloch-type transitions of domain walls [28,29].

Slightly above the ZZ instability the coupled equations (1),(2) can be reduced to the single equation

$$\partial_t\theta=D_1\partial_x^2\theta+D_y\partial_y^2\theta-D_4\partial_y^4\theta+\Gamma\partial_y(\partial_y\theta)^3 \qquad (37)$$

with $D_y=D_2(\mu-\mu_{zz})/|\mu_{zz}|$, $D_4=D_2K_2/|\mu zz|$, $\Gamma=(D_2/\nu)^2D_2g'/|\mu_{zz}|$. This weakly nonlinear description of the ZZ instability is valid for $\mu-\mu_{ZZ}/|\mu_{ZZ}|\ll 0$. Equation (37) is of very general importance. It describes the ZZ instability in anisotropic as well as isotropic media and by setting $a=\partial_y\theta$ it becomes the celebrated Cahn-Hilliard equation [26,30], which describes coarsening in systems with a conserved order parameter.

ACKNOWLEDGMENTS

We wish to thank W. Pesch, E. Plaut, A. G. Roßberg, and B. Dressel for valuable discussions and help. Financial support by the EU through TMR network Grant No. FMRX-CT96-0085 is gratefully acknowledged.

[1] H. Brand, C. Fradin, P. L. Finn, W. Pesch, and P. E. Cladis, Phys. Lett. A **235**, 502 (1997).
[2] P. Petrescu and M. Giurgea, Phys. Lett. **59A**, 41 (1976); L. Nasta, A. Lupu, and M. Giurgea, Mol. Cryst. Liq. Cryst. **71**, 65 (1981).
[3] L. Kramer and W. Pesch, in *Pattern Formation in Liquid Crystals*, edited by A. Buka and L. Kramer (Springer-Verlag, Berlin, 1996); W. Pesch and U. Behn, in *Evolution of Spontaneous Structures in Dissipative Continuous Systems*, edited by F. H. Busse and S. C. Müller (Springer-Verlag, Berlin, 1998).
[4] E. Braun, S. Rasenat, and V. Steinberg, Europhys. Lett. **15**, 597 (1991).
[5] S. Nasuno and S. Kai, Europhys. Lett. **14**, 779 (1991); S. Nasuno, O. Sasaki, S. Kai, and W. Zimmermann, Phys. Rev. A **46**, 4954 (1992).
[6] M. Kaiser and W. Pesch, Phys. Rev. E **48**, 4510 (1993).
[7] E. Plaut, W. Decker, A. Rossberg, L. Kramer, W. Pesch, A. Belaidi, and R. Ribotta, Phys. Rev. Lett. **79**, 2367 (1997).
[8] E. Plaut and W. Pesch, Phys. Rev. E **59**, 1747 (1999).
[9] The term ''abnormal rolls'' was introduced in the context of homeotropic convection, see H. Richter, A. Buka, and I. Rehberg, in *Spatio-Temporal Patterns in Nonequilibrium Complex Systems*, edited by P. E. Cladis and P. Palffy-Muhoray, (Addison-Wesley, Reading, MA, 1994).
[10] H. Amm, R. Stannarius, and A. G. Rossberg, Physica D **126**, 171 (1999).
[11] S. Rudroff, H. Zhao, L. Kramer, and I. Rehberg, Phys. Rev. Lett. **81**, 4144 (1998).
[12] M. Or-Guil, M. Bode, C. P. Schenk, and H.-G. Purwins, Phys. Rev. E **57**, 6432 (1998).
[13] S. Nasuno, O. Sasaki, S. Kai, and W. Zimmermann, Phys. Rev. A **46**, 4954 (1992).
[14] A. Belaidi, A. Joets, and R. Ribotta (unpublished); A. Belaidi, Ph.D. thesis, Université de Paris XI Orsay, Orsay, 1998.
[15] A. G. Rossberg, A. Hertrich, and W. Pesch, Phys. Rev. Lett. **76**, 4729 (1996); A. G. Roßberg and L. Kramer, Phys. Scr. **T67**, 121 (1996).
[16] A. G. Rossberg, Ph.D. thesis, Universität Bayreuth, Bayreuth, 1998.
[17] S. Rudroff, V. Frette, and I. Rehberg, Phys. Rev. E **59**, 1814 (1999).
[18] B. Dressel, E. Plaut, and W. Pesch (private communication).
[19] E. Ben-Jacob, H. Brand, G. Dee, L. Kramer, and J. S. Langer, Physica D **14**, 348 (1982); W. van Saarloos, Phys. Rev. A **39**, 6367 (1989).
[20] W. Pesch and L. Kramer, Z. Phys. B: Condens. Matter **63**, 121 (1986).
[21] P. Toth, A. Buka, J. Peinke, and L. Kramer, Phys. Rev. E **58**, 1983 (1998).
[22] J.-H. Huh, Y. Hidaka, and S. Kai, Phys. Rev. E **58**, 7355 (1998); J.-H. Huh, Y. Hidaka, A. G. Roßberg, and S. Kai, *ibid.* **61**, 2769 (2000).
[23] A. G. Rossberg, N. Eber, A. Buka, and L. Kramer, Phys. Rev. E **61**, R25 (2000).

[24] C. Fradin, P. L. Finn, H. R. Brand, and P. E. Cladis, Phys. Rev. Lett. **81**, 2902 (1998).
[25] Y. Gabune, J. Itona, and L. Liebert, J. Phys. (France) **49**, 681 (1988).
[26] C. Chevallard, M. Clerc, P. Coullet, and J. M. Gilli, Eur. Phys. J. E **1**, 179 (2000).
[27] H. Schmiedel, Ch. Cramer, R. Stannarius, K. Eidner, and M. Grigutsch, Liq. Cryst. **14**, 1935 (1993).
[28] P. Coullet, J. Lega, B. Houchmanzadeh, and J. Lajzerowicz, Phys. Rev. Lett. **65**, 1352 (1990).
[29] T. Frisch, S. Rica, P. Coullet, and J. M. Gilli, Phys. Rev. Lett. **72**, 1471 (1994).
[30] J. W. Cahn and J. E. Hilliard, J. Chem. Phys. **28**, 258 (1958).